CRYSTAL GROWTH & DESIGN

pubs.acs.org/crystal

Article

Combining Racetams with a Sweetener through Complexation

Published as part of a Crystal Growth and Design virtual special issue in Celebration of the Career of Roger Davey

Fucheng Leng, Koen Robeyns, Tom Leyssens,* and Oleksii Shemchuk

Cite This: *Cryst. Growth Des.* 2022, 22, 3016−3023

Read Online

ACCESS | Metrics & More | Article Recommendations | Supporting Information

ABSTRACT: Combining active pharmaceutical ingredients (APIs) with sweeteners through crystal engineering is an attractive way to mask the bitter taste of drugs. However, traditional methods such as salt or cocrystal formation still suffer some major limitations. Herein, racetams, a series of normally bitter drugs, cannot be combined with the popular sweetener saccharin through either salt or cocrystal formation. We here, however, show how these compounds can be combined when zinc saccharinate is used rather than saccharin. The obtained complexes can either be identified starting from a binary target API/Zn saccharinate or a ternary API/ZnO/saccharin combination. This work opens up novel pathways to couple two compounds of interest through a crystal engineering approach.

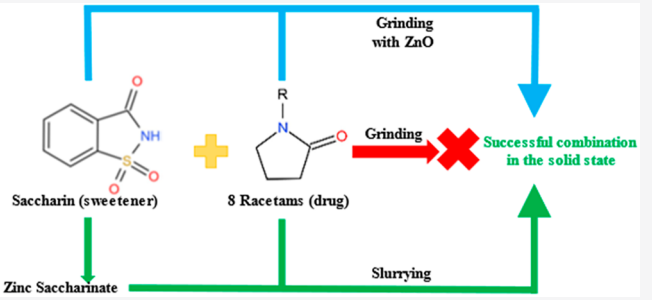

1. INTRODUCTION

Racetams are a series of active pharmaceutical ingredients (APIs) that impact the central nervous system.[1−4] Their unpleasant taste still is a hurdle in the development of their oral dosage forms.[5,6] For example, levetiracetam, marketed as Keppra, is used for the treatment of epilepsy.[7] Its intensively bitter taste usually leads to poor patient compliance, especially with children.[8,9] Similarly, piracetam, which has been marketed and used for the treatment of memory and balance problems,[10] met with the refusal of patients in clinical trials because of its bitter taste.[6]

Combining suitable sweeteners with racetams through crystal engineering is an attractive way to overcome such problems as they mask the bad taste of drug molecules but do not change their original chemical structure.[11−14] For drugs containing basic groups such as quinine, venlafaxine, haloperidol, stanozolol, lamivudine, triamterene, or mirtazapine, the acidic sweetener saccharin can easily be combined in the same solid form through the formation of salts.[15−19] For un-ionizable drugs, previous works have proven the possibility of combining sweeteners through cocrystallization.[20,21] For example, oxcarbazepine, spironolactone, and carbamazepine were cocrystallized with saccharin, a sweetener widely used in the pharmaceutical and food industry[22,23] with obtained solids showing improved solubility.[24−26] Albeit elegant, cocrystallization suffers from a low success rate in identifying suitable coformers.[27−29]

In this study, we introduce an innovative approach showing how saccharin can be successfully combined at the solid state with un-ionizable drug compounds for which no molecular cocrystals between drug and saccharin exist. Inspired by ionic cocrystallization,[30] we show how zinc saccharinate can be successfully combined with six racetams (Figure 1), which do not form a molecular cocrystal with saccharin. We, furthermore, highlight an efficient three-component grinding strategy for the identification of these complexes, which often show increased thermal stability with respect to the parent drug compound. The approach used in this work not only shows a novel way to combine sweeteners with drugs but also opens up a new perspective on how two target compounds can be combined at the solid state.

2. EXPERIMENTAL SECTION

2.1. Materials. Racetams, including levetiracetam, piracetam, oxiracetam, sunifiram, and carphedon, were purchased from Xiamen Top Health Biochem Tech. Co., Ltd. Etiracetam is the racemate of levetiracetam, which was obtained from the latter following a literature-based procedure.[31] Saccharin was purchased from Alfa Aesar. Zinc acetate was purchased from Carlroth. Zinc oxide was purchased from Merck. All of the solvents and reagents were used as received without further treatment.

2.2. Preparation of Zinc Saccharinate Hexahydrate [$ZnSac_2(H_2O)_4]\cdot 2H_2O$. $[ZnSac_2(H_2O)_4]\cdot 2H_2O$ (zinc saccharinate hereafter, Figure S1) was obtained by slurrying saccharin and zinc acetate in a

Received: December 13, 2021
Revised: April 13, 2022
Published: April 20, 2022

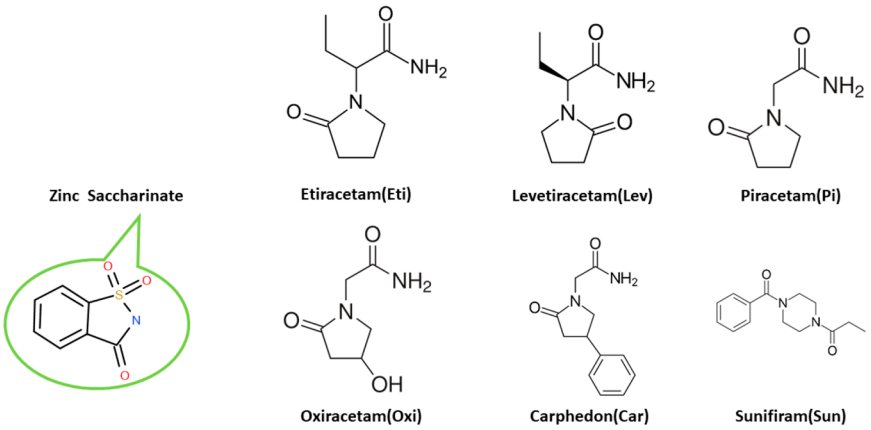

Figure 1. Zinc saccharinate and racetams used.

2:1 ratio in water at room temperature for 2 days. After that, the suspension was filtered, and the filtered cake collected and dried under ambient conditions.

2.3. Screening Procedure. *2.3.1. Three-Component Grinding.* Generally, 0.5 mmol of saccharin, 0.25 mmol of ZnO, 0.25 mmol of racetam, and 2−3 stainless metal balls (Ø 3 mm) were added to a plastic Eppendorf tube. After 40 μL of solvent (methanol, ethanol, isopropanol, acetonitrile, or water) was added, the samples were ground in a RETSCH Mixer Mill MM 400 with a beating frequency of 30 Hz for 90 min. The PXRD profiles of the resulting powders were compared to the parent compounds as well as the different zinc saccharinate solvates.

2.3.2. Two-Component Grinding. For levetiracetam, two-component grinding is performed starting directly from zinc saccharinate. A total of 0.1 mmol of zinc saccharinate, 0.1 mmol of levetiracetam, and three stainless-steel balls were added to a plastic Eppendorf tube. After 20 μL of solvent (methanol, ethanol, isopropanol, acetonitrile, or water) was added, samples were ground using a RETSCH Mixer Mill MM 400 with a beating frequency of 30 Hz for 90 min. The PXRD profiles were compared to those of the parent compounds as well as all zinc saccharinate solvates (Table S1).

2.4. Single Crystal Growth. *2.4.1. $ZnSac_2Lev$, $ZnSac_2Eti_2$, $[ZnSac_2Pi]\cdot CH_3CN$, $[ZnSac_2Oxi]\cdot CH_3CN$, $[ZnSac_2Sun]\cdot CH_3CN$.* These were obtained following a similar procedure: to 0.1 mmol of zinc saccharinate and the corresponding racetams, 1 mL of acetonitrile was added, and the solution was heated to 80 °C. Afterward, seeds of the respective complexes obtained from grinding were added to the solution, and the glass vial was sealed and left to cool down slowly overnight.

2.4.2. $[ZnSac_2(H_2O)_2]\cdot Car\cdot EtOH\cdot H_2O$ and $Zn_3Sac_6Pi_2(H_2O)_4$. These were obtained following the procedure in section 2.4.1, apart from using a water−ethanol mixture (0.05:0.95 in volume) instead of acetonitrile.

2.4.3. $[ZnSac_2Lev(H_2O)]\cdot EtOH$. To a physical mixture of 0.1 mmol of zinc saccharinate and 0.4 mmol of levetiracetam, ethanol was added dropwise until all solid was dissolved. Single crystals of $[ZnSac_2Lev(H_2O)]\cdot EtOH$ were obtained after leaving the solution to partially evaporate after 1 day.

2.4.4. $[ZnSac_2Lev(H_2O)]\cdot CH_3CN$. A total of 0.1 mmol of zinc saccharinate was dissolved in 1 mL of acetonitrile by heating. The obtained solution was mixed with an equimolar quantity of levetiracetam dissolved in 1 mL of acetonitrile at RT. The solution was kept at 9 °C, and single crystals suitable for structure determination were collected after 24 h.

2.4.5. $ZnSac_2Car$. A total of 0.1 mmol of zinc saccharinate and 0.1 mmol of carphedon were stirred in 2 mL of ethanol for 2 h. Afterward, the solution was heated to 85 °C. At this temperature, ethanol was added dropwise until all solids were dissolved. Seeds, obtained from grinding experiments, were added to the solution. The glass vial was sealed and left to cool down slowly overnight, after which single crystals were harvested.

2.5. Powder X-ray Diffraction (PXRD) and Variable-Temperature X-ray Powder Diffraction (VT-PXRD). Powder X-ray diffraction of all samples were conducted on a Siemens D5000 diffractometer equipped with a Cu X-ray source operating at 40 kV and 40 mA (λ = 1.5418 Å) at a scanning range of 2θ values from 5° to 50° at a scan rate of 0.6° min^{-1}. VT-XRPD profiles were collected on a PANalytical X'Pert PRO automated diffractometer at a scanning range of 2θ values from 3° to 40°, equipped with an X'Celerator detector and an Anton Paar TTK 450 system for measurements at a controlled temperature. Data were collected in the open air in Bragg−Brentano geometry, using Cu−Kα radiation without a monochromator.

2.6. Single-Crystal Diffraction. Data were collected on a MAR345 image plate detector using Mo Kα radiation (λ = 0.71073 Å), generated by an Incoatec IμS microfocus source. Data integration and reduction were performed by CrystAlis^{PRO}, and the implemented absorption correction was applied. Structure solution was performed by the dual-space algorithm in SHELXT, and the structure was further refined against F^2 using SHELXL.[32] All non-hydrogen atoms were refined anisotropically, and hydrogen atoms were placed at calculated positions with temperature factors set at 1.2U_{eq} of the parent atoms (1.5U_{eq} for methyl and OH hydrogens).

2.7. Thermogravimetric Analysis (TGA). TGA analyses of all samples were performed from 30 to 500 °C using a heating rate of 10 °C/min with a continuous nitrogen flow of 50 mL/min, on a Mettler Toledo TGA/SDTA851e.

2.8. Differential Scanning Calorimetry (DSC). DSC measurements were performed on a TA DSC2500. Deposited in aluminum Tzero pans with punctured lids, samples were heated from 20 °C up to 350 °C using a heating rate of 10 °C/min under a 50 mL/min continuous nitrogen flow.

3. RESULTS AND DISCUSSION

3.1. The Unexplored Potential of Using Complexation to Bind a Drug and a Sweetener. Because of the lack of ionizable groups in all investigated racetams (Figure 1), combining them with saccharin through salt formation is not possible. On top of that, all attempts to directly cocrystallize saccharin with these racetams were unsuccessful. This failure in cocrystallization can be explained by the fact that the intermolecular interactions in the expected cocrystals are of the same type as those in the starting compounds (hydrogen bonding, $\pi-\pi$ interactions...) but overall less favorable for the potential cocrystal compared to the starting compounds. Aiming for a stronger stabilization of the resulting crystalline solid, we focused on inducing stronger interactions. Recently,

https://doi.org/10.1021/acs.cgd.1c01462
Cryst. Growth Des. 2022, 22, 3016−3023

ionic cocrystals have emerged showing stronger interactions between the metal center and the organic compounds, resulting often in a higher success rate to cocrystal formation.[31,33−35] Unlike molecular cocrystals, the dominating force that combines different compounds together is not hydrogen bonding or $\pi-\pi$ stacking, but rather coordination and electrostatic interactions, which are much stronger.[30] Considering zinc is pharmaceutically acceptable and its inorganic salt was shown to cocrystallize with different racetams,[28,36] we took an innovative approach, converting saccharin to zinc saccharinate and using this latter to form complexes combining both saccharin as well as the target API.

3.2. Mechanochemical Strategies. Previous contributions in metallopharmaceuticals have shown the effectiveness of mechanochemistry in finding metal complexes.[37,38] In our case, saccharin shows a pK_a of 1.6 and easily deprotonates.[27] The most obvious method here would be to convert saccharin to the zinc saccharinate salt. This salt can then be ground with the API, to screen for complex formation (two-component grinding). Although successful, the supplementary synthetic step of synthesizing the zinc saccharinate salt makes this procedure lengthy and time-consuming. However, as liquid-assisted grinding (LAG) has already proven capable of promoting the reaction between metal oxides and organic acids in a one-step synthesis of multiple ligand complexes,[39−41] a similar approach proved successful here. The combination of saccharin, zinc oxide, and API in a single-step grinding approach yielded the desired complexes (three-component grinding).

To evaluate the usefulness of both grinding approaches, a series of two- and three-component grinding experiments were performed for the mechanochemical coupling of levetiracetam, zinc, and saccharin. This highlighted the importance of the solvent used during the grinding experiments. In all cases, neat grinding failed to yield the desired complexes: the mixture of starting materials was observed for both two- and three-component grinding experiments even after 90 min of milling. A similar observation was made by Chow et al. working on magnesium oxide (Figures S2−S3).[41]

LAG using water also did not lead to successful transformation for the two- as well as the three-component grinding experiments. In both cases, a mixture of the zinc saccharinate hexahydrate and levetiracetam was obtained (Figure S4). This can be explained as the stability of zinc saccharinate hexahydrate is directly related to the water activity (eq 1). whereas high water activity leads to the formation of levetiracetam physically mixed with zinc saccharinate hexahydrate. Water-assisted LAG can be assimilated to the highest water activity under which the equilibrium is completely shifted to the hexahydrate phase.

$$[ZnSac_2(H_2O)_4]\cdot 2H_2O_{solid} + Lev_{solid} \rightleftharpoons ZnSac_2Lev_{solid} + 6H_2O_{liquid} \quad (1)$$

LAG using organic solvents (Figure S5) leads to a reduced overall water activity, pulling the reaction toward the formation of the various desired complexes. As the use of 2 equiv of saccharin and 1 equiv of ZnO during the three-component grinding only introduces one equivalent of water (the only water introduced in the reaction is obtained as byproduct of two saccharin molecules with zinc oxide) versus the 6 equiv introduced when performing the two-component grinding using zinc saccharinate hexahydrate, the transformation is more advanced, as shown by the weaker peaks from the zinc saccharinate residue in the three-component grinding experiments compared to two-component grinding experiments (Figures S6−S8). Furthermore, to our surprise, different patterns appeared when using methanol, ethanol, and acetonitrile, which were shown to correspond to unsolvated form $ZnSac_2Lev$ and the solvated form of the complex containing one molecule of water and one molecule of solvent ($ZnSac_2Lev(H_2O)\cdot EtOH$ and $ZnSac_2Lev(H_2O)\cdot CH_3CN$ respectively) (Table S2, Figures S9−S11). This result shows the importance of the solvent used during LAG and highlights the crucial role of the water activity when hydrates are involved in the transformation process. It should be mentioned that compared to the hydrate and anhydrate phases, these solvate phases are less interesting from a pharmaceutical point of view.

On the basis of the results above, the three-component liquid-assisted grinding using organic solvents was opted as the principal approach for the coupling of the other racetams to saccharin.

3.3. Saccharinate-Zn-Racetam Complexes. To our astonishment, the coupling of zinc saccharinate and racetams at the solid state was successfully achieved for the six racetams studied here, through three-component grinding. This is in strong contrast to the direct coupling attempts between saccharin and racetams, which all failed (Figures S6−S8 and S12−S19).

To gain structural insight into how racetams couple to zinc saccharinate, a series of single crystals were grown. Considering most racetams share common structural motifs, one could reasonably expect some likeness in the crystal structures of the obtained complexes. In most complexes, zinc shows a tetrahedral coordination involving the nitrogen atoms of two saccharinate anions and two oxygen atoms of respectively a pyrrolidone and amide group of two different racetam molecules (Figure 2). As for each racetam molecule, the

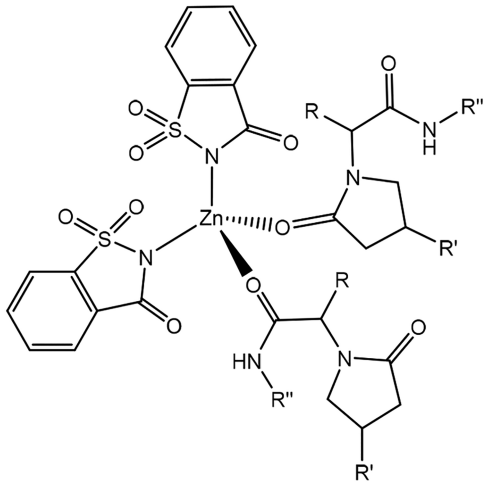

Figure 2. The most common coordination environment around Zn^{2+} in the obtained complexes.

pyrrolidone and amide group link to two different zinc atoms, and an infinite 1D chain structure or 0D complex is formed. This coordination mode is observed in $ZnSac_2Lev$, $ZnSac_2Car$, $[ZnSac_2Pi]\cdot CH_3CN$, $[ZnSac_2Oxi]\cdot CH_3CN$, and $[ZnSac_2Sun]\cdot CH_3CN$ complexes. $ZnSac_2Lev$ is shown here, while the other complexes are shown in the Supporting Information (Figure 2, Figures 3a and S20−S24, Tables S2−S3).

https://doi.org/10.1021/acs.cgd.1c01462
Cryst. Growth Des. 2022, 22, 3016−3023

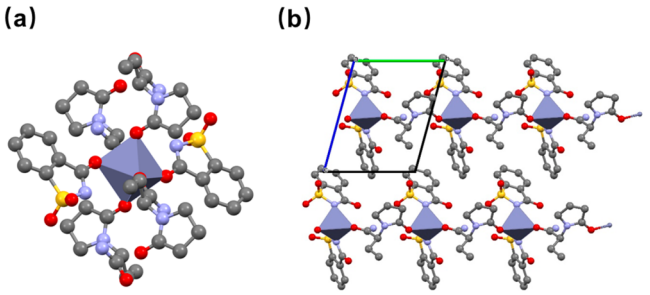

Figure 3. (a) The coordination environment of Zn^{2+} in $ZnSac_2Lev$. (b) Crystal packing of $ZnSac_2Lev$, view along the crystallographic *a*-axis. Hydrogen atoms are omitted for clarity.

$ZnSac_2Lev$, $ZnSac_2Eti_2$, $[ZnSac_2Lev(H_2O)]\cdot EtOH$, $[ZnSac_2Lev(H_2O)]\cdot CH_3CN$, $Zn_3Sac_6Pi_2(H_2O)_4$, and $[ZnSac_2(H_2O)_2]\cdot Car\cdot EtOH\cdot H_2O$ show different coordination modes around the zinc cation, which is why these structures are discussed in more detail, keeping in mind the tetrahedral coordination mentioned above is most frequent.

Upon attempting to obtain single crystals of the complexes, four new solvates of zinc saccharinate were discovered and structurally characterized: $[Zn(Sac)_2(MeOH)_2]$, $[Zn(Sac)_2(EtOH)_2]$ $[Zn(Sac)_2(isopropanol)(H_2O)]$, and $[ZnSac_2(CH_3CN)(H_2O)]$ (Table S1).

3.3.1. Complexation with Levetiracetam. Three different solid forms involving complexation of zinc saccharinate with levetiracetam were identified in this work. $ZnSac_2Lev$, $[ZnSac_2Lev(H_2O)]\cdot EtOH$, and $[ZnSac_2Lev(H_2O)]\cdot CH_3CN$ (Figures S5−S8) were accessed mechanochemically, and single crystals of these phases were identified.

3.3.1.1. $ZnSac_2Lev$. $ZnSac_2Lev$ adopts a tetrahedral coordination leading to the 1D coordination mode mentioned above, in which every two adjacent zinc atoms are bridged by one levetiracetam molecule (Figure 3). $ZnSac_2Lev$ can be obtained through three-component LAG using methanol or isopropanol or by slurrying zinc saccharinate and levetiracetam in isopropanol in a 1:1.2 ratio (Figures S9 and S25).

In addition, $ZnSac_2Lev$ shows considerable thermal stability compared to levetiracetam (levetiracetam shows a melting point of 116 °C). TGA analysis shows a rapid mass decline starting from 220 °C, corresponding to the single endothermic peak at 243 °C in the DSC thermogram, demonstrating the melting and further decomposition of the complex (Figure 4).

3.3.1.2. $[ZnSac_2Lev(H_2O)]\cdot CH_3CN$ and $[ZnSac_2Lev(H_2O)]\cdot EtOH$. Both solvated complexes share a similar coordination sphere around the zinc cation (Figure 5a). Once again, zinc

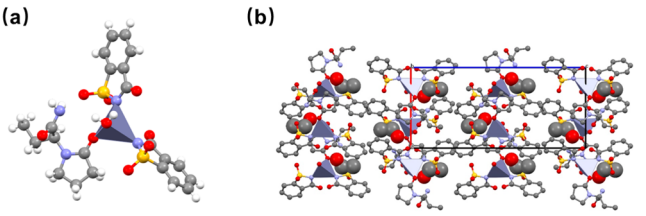

Figure 5. (a) The coordination environment of zinc in $[ZnSac_2Lev(H_2O)]\cdot EtOH$. (b) Crystal packing of $[ZnSac_2Lev(H_2O)]\cdot EtOH$ viewed along the crystallographic *a*-axis. Hydrogen atoms are omitted for clarity.

accepts a tetrahedral coordination formed by two nitrogen atoms from saccharinate and two oxygen atoms. However, while in $ZnSac_2Lev$ both oxygens of levetiracetam are involved in the complexation to Zn^{2+}, resulting in the infinite 1D chain formation, in the solvated complexes only the oxygen of pyrrolidone is bound to the cation, resulting in 0D complexes. In both solvates, a water molecule coordinates to the cation instead of the oxygen of the amide group. This latter interacts with adjacent molecules via $OH_{water}\cdots O_{amide}$ and $NH_{amide}\cdots O_{SO}$ hydrogen bonds (Figure 5b, Figure S24). Thus, $[ZnSac_2Lev(H_2O)]\cdot CH_3CN$ and $[ZnSac_2Lev(H_2O)]\cdot EtOH$ can be considered as acetonitrile and ethanol solvates of $ZnSac_2Lev(H_2O)$ respectively (Figure 5, Figure S24). Both complexes can be obtained in bulk using three-component acetonitrile or ethanol LAG or alternatively slurrying a stoichiometric ratio of zinc saccharinate and levetiracetam in acetonitrile or ethanol (Figures S10, S11, S26, and S27).

Thermal analysis of $[ZnSac_2Lev(H_2O)]\cdot CH_3CN$ shows an 8% weight loss starting from 75 °C, which can be attributed to the loss of acetonitrile and water (theoretical weight loss = 7.8%). This endothermic event is also visible in the DSC thermogram (Figure. 6). After this endothermic signal, a further single endothermal peak is seen at 241 °C, which corresponds to the melting of $ZnSac_2Lev$ (243 °C). VT-PXRD shows the solvent loss to lead to the unsolvated $ZnSac_2Lev$

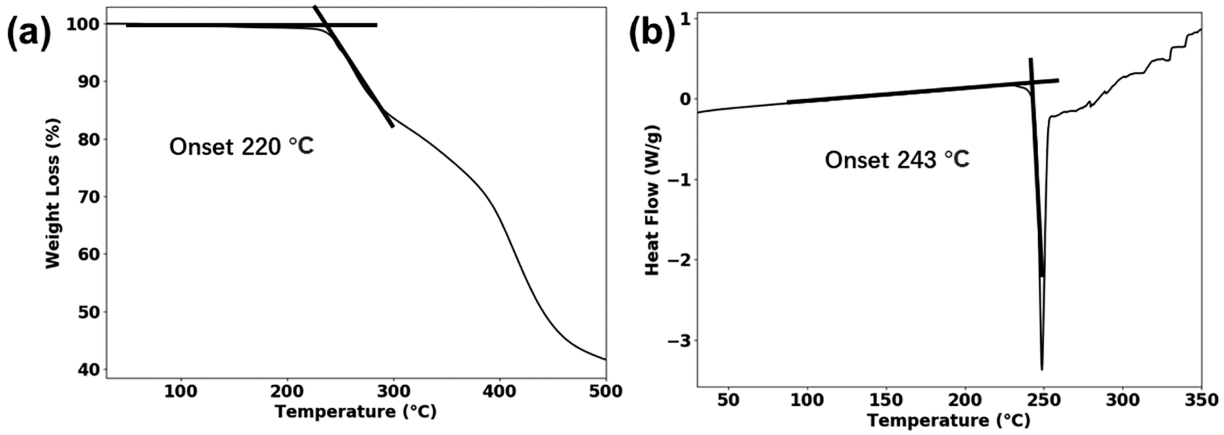

Figure 4. (a) TGA curve of $ZnSac_2Lev$. (b) DSC curve of $ZnSac_2Lev$.

https://doi.org/10.1021/acs.cgd.1c01462
Cryst. Growth Des. 2022, 22, 3016−3023

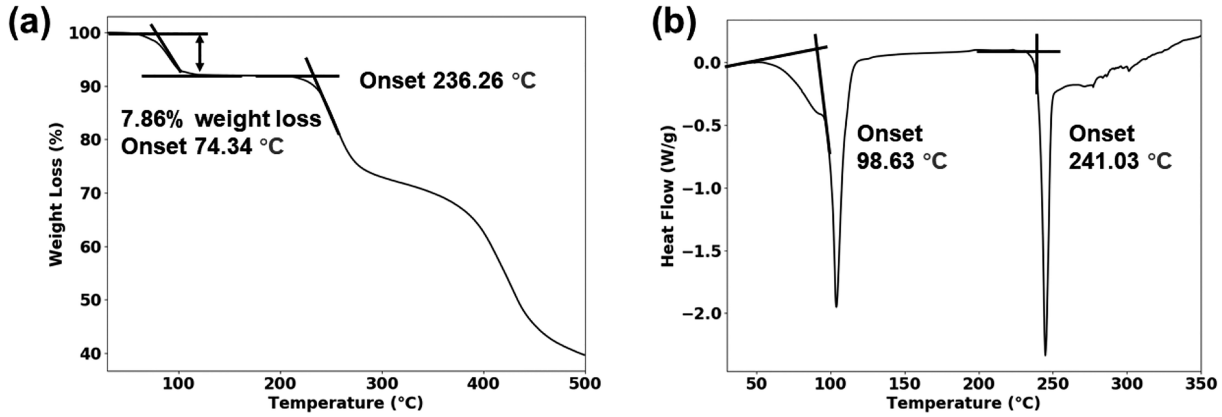

Figure 6. (a) TGA curve of $[ZnSac_2Lev(H_2O)]\cdot CH_3CN$. (b) TGA curve of $[ZnSac_2Lev(H_2O)]\cdot CH_3CN$.

complex (Figure S28) $[ZnSac_2Lev(H_2O)]\cdot EtOH$ shows a similar thermal behavior. The 8.44% weight loss starts from about 69 °C, corresponding to the first endothermal peak of the DSC curve. After the solvent loss, $[ZnSac_2Lev(H_2O)]\cdot EtOH$ is transformed to $ZnSac_2Lev$, which melts at about 236 °C, comparable to the measured melting point of $ZnSac_2Lev$ (243 °C) (Figures S29–S31).

3.3.2. Complexation with Etiracetam. Complexation of levetiracetam's racemic counterpart, etiracetam, did not show any solvate formation, resulting in the formation of $ZnSac_2Eti_2$, which crystallizes in a $P2_1/c$ space group. Unlike the majority of complexes obtained, an octahedral coordination is observed around the zinc cation. $ZnSac_2Eti_2$ can furthermore be regarded as a 1D coordination polymer with etiracetam molecules bridging two zinc cations (Figure 7). Two etiracetam molecules coordinating to two adjacent cations act as a bridge through their pyrrolidone and amide groups. The octahedral coordination is fulfilled by two saccharinate anions through the carbonyl oxygen instead of the nitrogen atoms unlike all other complexes obtained. This is a rare occurrence for this type of coordination involving saccharinate, as a CSD search confirms that nitrogen coordination is more likely.[42−44] Each zinc cation coordinates two etiracetam molecules of opposite chirality. The strands are therefore heterochiral, with no chiral recognition occurring for this compound.

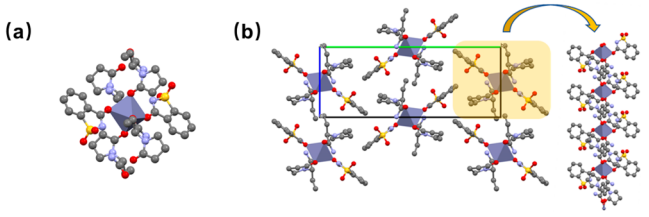

Figure 7. $ZnSac_2Eti_2$. (a) The coordination environment of zinc; (b) crystal packing, view along the crystallographic *a*-axis and the one-dimensional chain. Hydrogen atoms are omitted for clarity.

The simulated PXRD pattern overlaps with that of the ground material (Figure S32), showing the same phase was obtained. In addition, the synthesis of Sac_2ZnEti_2 was upscaled by slurrying stoichiometric amounts of zinc saccharinate and etiracetam in ethanol or isopropanol (Figure S33).

Thermal analysis (DSC and TGA) of $ZnSac_2Eti_2$ shows a single melting endotherm at 189 °C followed by immediate degradation (Figure 8). The introduction of zinc saccharinate thermally stabilizes etiracetam in the solid state by about 70 °C (etiracetam shows a melting point of 119 °C).[45] Merely cocrystallizing etiracetam with $ZnCl_2$ shows almost no increase of etiracetam's melting point (around 118 °C), highlighting the importance of saccharinate in this stabilization.[36]

3.3.3. Complexation with Piracetam. Complexation of piracetam with zinc saccharinate always resulted in the formation the hydrated $Zn_3Sac_6Pi_2(H_2O)_4$ complex regardless

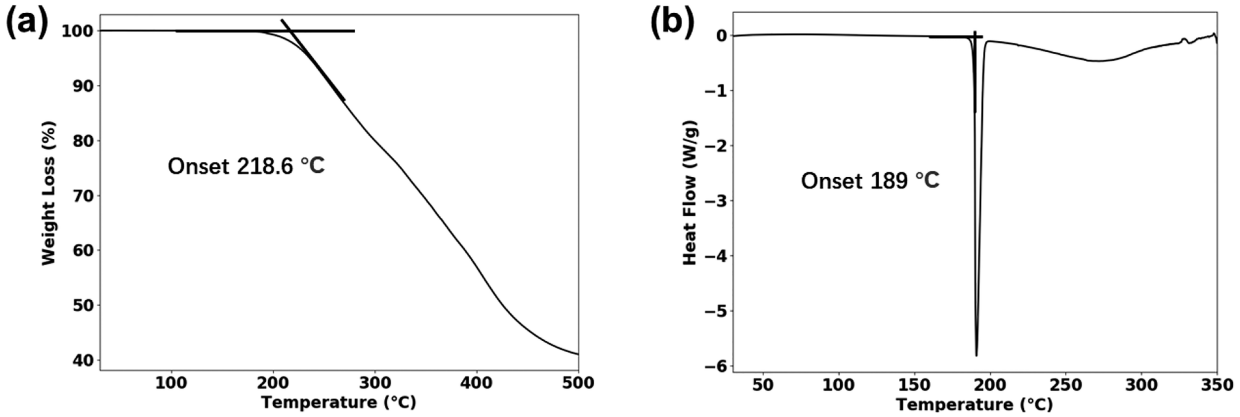

Figure 8. (a) TGA curve of $ZnSac_2Eti_2$ and (b) DSC curve of $ZnSac_2Eti_2$.

https://doi.org/10.1021/acs.cgd.1c01462
Cryst. Growth Des. 2022, 22, 3016−3023

of the synthetic method (LAG or slurrying in ethanol, acetonitrile, or isopropanol (Figures S34–S35).

The structure of $Zn_3Sac_6Pi_2(H_2O)_4$ differs significantly from the other complexes (Figure 9). First, the stoichiometric ratio

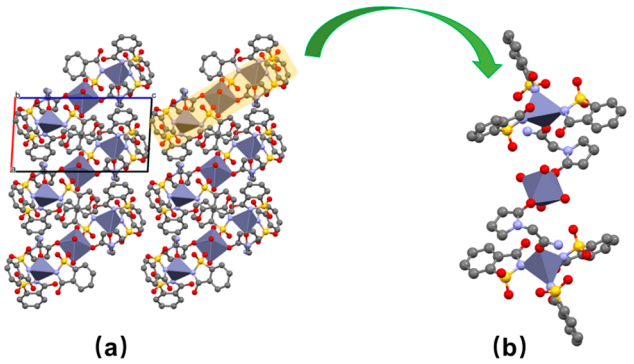

Figure 9. (a) Crystal packing of $Zn_3Sac_6Pi_2(H_2O)_4$, viewed along the crystallographic *b*-axis. The yellow rectangle represents one $Zn_3Sac_6Pi_2(H_2O)_4$ monomer (b). $Zn_3Sac_6Pi_2(H_2O)_4$ monomer structure.

of zinc saccharinate to piracetam is different, showing a 3:2 instead of the most common 1:1 ratio. Second, this complex is characterized by both tetrahedral as well as octahedral coordination around the zinc cation. Two zinc cations have a tetrahedral coordination formed by three nitrogen atoms of saccharinate and an oxygen from a piracetam amide group. The pyrrolidone oxygens of piracetam, in turn, are coordinated to the octahedrally coordinated zinc cation which is situated in between the above-mentioned tetrahedra. The octahedral coordination is completed by four water molecules. This combination of tetra- and octahedrally coordinated zinc leads to a $Zn_3Sac_6Pi_2(H_2O)_4$ monomer. These monomers interact with each other via hydrogen bonds between the water molecules and amide group of piracetam and oxygen atoms of saccharinate (Figure. 9a).

3.3.4. Complexation with Carphedon. The complexation of zinc saccharinate with carphedon revealed a unique molecular cocrystal $[ZnSac_2(H_2O)_2]\cdot Car\cdot EtOH\cdot H_2O$, which can be obtained by slurrying or LAG methods using ethanol as a solvent (Figures S36 and S37). $[ZnSac_2(H_2O)_2]\cdot Car\cdot EtOH\cdot H_2O$ is the only complex in which the racetam compound is not coordinated to the zinc cation. The tetrahedral coordination of Zn^{2+} is formed by two saccharinate and two water molecules (Figure 10a), with carphedon interacting with

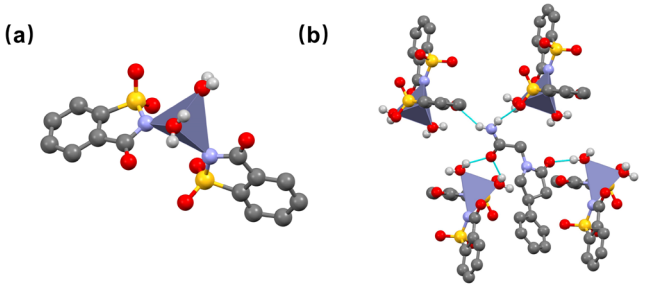

Figure 10. (a) The coordination environment of Zn^{2+}; (b) hydrogen bonding interaction between carphedon and $[ZnSac_2(H_2O)_2]$. H_{CH} atoms were omitted for the sake of clarity.

the $[ZnSac_2(H_2O)_2]$ motif through hydrogen bonding (Figure 10b). $[ZnSac_2(H_2O)_2]\cdot Car\cdot EtOH\cdot H_2O$ can therefore be described as a solvated cocrystal between $[ZnSac_2(H_2O)_2]$ and carphedon.

4. CONCLUSION

This paper introduces a novel methodology to couple a sweetener to a drug compound, as demonstrated for the racetam family. Whereas salt or cocrystal formation between the sweetener saccharin and racetams is not feasible, they can however be coupled together at the solid state, complexing the racetam compound with zinc saccharinate. We successfully applied this methodology to 6 different racetams, leading to 10 solid forms structurally identified in this paper. Interestingly, various structural features occur for these complexes with tetrahedral as well as octahedral coordination modes around the zinc cation, for which well-chosen examples of the various cases are presented here. Furthermore, the solid-state landscape can be expanded through the existence of various solvates of the obtained complexes, involving water as well as organic solvents. This shows the complexity surrounding these complexes, rendering the prediction of their structural assembly nontrivial. Despite the large variety in structural features, all complexes remained stable under ambient conditions and can easily be obtained through mechanochemical or solution-based methodologies, all showing increased thermal stability.

This methodology can easily be transposed to other systems for which cocrystallization between the target compound and the coformer (a sweetener in our case) cannot be achieved, once more expanding the solid-state landscape of target compounds.

■ ASSOCIATED CONTENT

Supporting Information

The Supporting Information is available free of charge at https://pubs.acs.org/doi/10.1021/acs.cgd.1c01462.

Additional PXRD pattern, thermal analysis results, and crystallography table (PDF)

Accession Codes

CCDC 2127927–2127940 contain the supplementary crystallographic data for this paper. These data can be obtained free of charge via www.ccdc.cam.ac.uk/data_request/cif, or by emailing data_request@ccdc.cam.ac.uk, or by contacting The Cambridge Crystallographic Data Centre, 12 Union Road, Cambridge CB2 1EZ, UK; fax: +44 1223 336033.

■ AUTHOR INFORMATION

Corresponding Author

Tom Leyssens − *Institute of Condensed Matter and Nanosciences, UCLouvain, 1348 Louvain-La-Neuve, Belgium;* orcid.org/0000-0001-7916-1373; Email: tom.leyssens@uclouvain.be

Authors

Fucheng Leng − *Institute of Condensed Matter and Nanosciences, UCLouvain, 1348 Louvain-La-Neuve, Belgium*

Koen Robeyns − *Institute of Condensed Matter and Nanosciences, UCLouvain, 1348 Louvain-La-Neuve, Belgium;* orcid.org/0000-0002-4763-4217

Oleksii Shemchuk − *Institute of Condensed Matter and Nanosciences, UCLouvain, 1348 Louvain-La-Neuve, Belgium;* orcid.org/0000-0003-3003-3922

Complete contact information is available at: https://pubs.acs.org/10.1021/acs.cgd.1c01462

Notes

The authors declare no competing financial interest.

■ ACKNOWLEDGMENTS

F.L. would like to thank the China Scholarship Council (CSC) for financial support.

■ REFERENCES

(1) Spignoli, G.; Pepeu, G. Interactions between oxiracetam, aniracetam and scopolamine on behavior and brain acetylcholine. *Pharmacol., Biochem. Behav.* **1987**, *27* (3), 491−495.
(2) Ghelardini, C.; Galeotti, N.; Gualtieri, F.; Manetti, D.; Bucherelli, C.; Baldi, E.; Bartolini, A. DM235 (sunifiram): a novel nootropic with potential as a cognitive enhancer. *Naunyn Schmiedebergs Arch. Pharmacol.* **2002**, *365* (6), 419−426.
(3) Löscher, W.; Richter, A. Piracetam and levetiracetam, two pyrrolidone derivatives, exert antidystonic activity in a hamster model of paroxysmal dystonia. *Eur. J. Pharmacol.* **2000**, *391* (3), 251−254.
(4) Malykh, A. G.; Sadaie, M. R. J. D. Piracetam and piracetam-like drugs. *Drugs* **2010**, *70* (3), 287−312.
(5) Kavanagh, O. N.; Wang, C.; Walker, G. M.; Sun, C. C. Modulation of the powder properties of lamotrigine by crystal forms. *Int. J. Pharm.* **2021**, *595*, 120274.
(6) Pranzatelli, M. R.; Tate, E. D.; Galvan, I.; Wheeler, A. Controlled pilot study of piracetam for pediatric opsoclonus-myoclonus. *Clin Neuropharmacol* **2001**, *24* (6), 352−357.
(7) Hovinga, C. A. Levetiracetam: a novel antiepileptic drug. *Pharmacotherapy* **2001**, *21* (11), 1375−1388.
(8) Sivaneswari, S.; Karthikeyan, E.; Veena, D.; Chandana, P. J.; Sai Sumana, P.; Subhashree, P.; Ramya, R.; Rajalakshmi, L.; Ashok Kumar, C. K. Physiochemical characterization of taste masking levetiracetam ion exchange resinates in the solid state and formulation of stable liquid suspension for pediatric use. *Beni-Suef University Journal of Basic and Applied Sciences* **2016**, *5* (2), 126−133.
(9) Crepeau, A. Z.; Treiman, D. M. Levetiracetam: a comprehensive review. *Expert Review of Neurotherapeutics* **2010**, *10* (2), 159−171.
(10) Winblad, B. Piracetam: a review of pharmacological properties and clinical uses. *CNS Drug Rev.* **2005**, *11* (2), 169−182.
(11) Karimi-Jafari, M.; Padrela, L.; Walker, G. M.; Croker, D. M. Creating Cocrystals: A Review of Pharmaceutical Cocrystal Preparation Routes and Applications. *Cryst. Growth Des.* **2018**, *18* (10), 6370−6387.
(12) Sun, C. C. Cocrystallization for successful drug delivery. *Expert Opin Drug Deliv* **2013**, *10* (2), 201−213.
(13) Bhatt, P. M.; Ravindra, N. V.; Banerjee, R.; Desiraju, G. R. Saccharin as a salt former. Enhanced solubilities of saccharinates of active pharmaceutical ingredients. *Chem. Commun. (Camb)* **2005**, *8*, 1073−1075.
(14) Blagden, N.; de Matas, M.; Gavan, P. T.; York, P. Crystal engineering of active pharmaceutical ingredients to improve solubility and dissolution rates. *Adv. Drug Deliv Rev.* **2007**, *59* (7), 617−630.
(15) Liu, S.; Wang, C.; Chen, H.; Sun, C. C. Sweet Sulfamethazine Acesulfamate Crystals with Improved Compaction Property. *Cryst. Growth Des.* **2021**, *21* (2), 1077−1085.
(16) Kong, M.; Fu, X.; Li, J.; Li, J.; Chen, M.; Deng, Z.; Zhang, H. Sweet pharmaceutical salts of stanozolol with enhanced solubility and physical stability. *CrystEngComm* **2016**, *18* (45), 8739−8746.
(17) Banerjee, R.; Bhatt, P. M.; Ravindra, N. V.; Desiraju, G. R. Saccharin Salts of Active Pharmaceutical Ingredients, Their Crystal Structures, and Increased Water Solubilities. *Cryst. Growth Des.* **2005**, *5* (6), 2299−2309.
(18) Martins, F. T.; Paparidis, N.; Doriguetto, A. C.; Ellena, J. Crystal Engineering of an Anti-HIV Drug Based on the Recognition of Assembling Molecular Frameworks. *Cryst. Growth Des.* **2009**, *9* (12), 5283−5292.
(19) Li, A.-Y.; Xu, L.-L.; Chen, J.-M.; Lu, T.-B. Solubility and Dissolution Rate Enhancement of Triamterene by a Cocrystallization Method. *Cryst. Growth Des.* **2015**, *15* (8), 3785−3791.
(20) Basavoju, S.; Bostrom, D.; Velaga, S. P. Indomethacin-saccharin cocrystal: design, synthesis and preliminary pharmaceutical characterization. *Pharm. Res.* **2008**, *25* (3), 530−541.
(21) Hou, X.; Feng, Y.; Zhang, P.; Wei, H.; Dang, L. Selective Crystal Growth of Theophylline-Saccharin Cocrystal on Self-Assembled Monolayer from Incongruent System. *Cryst. Growth Des.* **2015**, *15* (10), 4918−4924.
(22) Zhao, X.; Li, Q.; Wang, C.; Hu, S.; He, X.; Sun, C. C. Simultaneous taste-masking and oral bioavailability enhancement of Ligustrazine by forming sweet salts. *Int. J. Pharm.* **2020**, *577*, 119089.
(23) Chattopadhyay, S.; Raychaudhuri, U.; Chakraborty, R. Artificial sweeteners - a review. *J. Food Sci. Technol.* **2014**, *51* (4), 611−621.
(24) Takata, N.; Takano, R.; Uekusa, H.; Hayashi, Y.; Terada, K. A Spironolactone−Saccharin 1:1 Cocrystal Hemihydrate. *Cryst. Growth Des.* **2010**, *10* (5), 2116−2122.
(25) Hickey, M. B.; Peterson, M. L.; Scoppettuolo, L. A.; Morrisette, S. L.; Vetter, A.; Guzman, H.; Remenar, J. F.; Zhang, Z.; Tawa, M. D.; Haley, S. Performance comparison of a co-crystal of carbamazepine with marketed product. *Eur. J. Pharm. Biopharm* **2007**, *67* (1), 112−119.
(26) Chadha, R.; Saini, A.; Jain, D. S.; Venugopalan, P. Preparation and Solid-State Characterization of Three Novel Multicomponent Solid Forms of Oxcarbazepine: Improvement in Solubility through Saccharin Cocrystal. *Cryst. Growth Des.* **2012**, *12* (8), 4211−4224.
(27) Wang, C.; Perumalla, S. R.; Sun, C. C. Anion Exchange Reaction for Preparing Acesulfame Solid Forms. *Cryst. Growth Des.* **2018**, *18* (8), 4215−4219.
(28) Buol, X.; Robeyns, K.; Caro Garrido, C.; Tumanov, N.; Collard, L.; Wouters, J.; Leyssens, T. Improving Nefiracetam Dissolution and Solubility Behavior Using a Cocrystallization Approach. *Pharmaceutics* **2020**, *12* (7), 653.
(29) Leng, F.; Robeyns, K.; Leyssens, T. Urea as a Cocrystal Former-Study of 3 Urea Based Pharmaceutical Cocrystals. *Pharmaceutics* **2021**, *13* (5), 671.
(30) Braga, D.; Grepioni, F.; Shemchuk, O. Organic−inorganic ionic co-crystals: a new class of multipurpose compounds. *CrystEngComm* **2018**, *20* (16), 2212−2220.
(31) Song, L.; Shemchuk, O.; Robeyns, K.; Braga, D.; Grepioni, F.; Leyssens, T. Ionic Cocrystals of Etiracetam and Levetiracetam: The Importance of Chirality for Ionic Cocrystals. *Cryst. Growth Des.* **2019**, *19* (4), 2446−2454.
(32) Sheldrick, G. M. Crystal structure refinement with SHELXL. *Acta Crystallogr. C Struct Chem.* **2015**, *71* (1), 3−8.
(33) Shemchuk, O.; Spoletti, E.; Braga, D.; Grepioni, F. Solvent Effect on the Preparation of Ionic Cocrystals of dl-Amino Acids with Lithium Chloride: Conglomerate versus Racemate Formation. *Cryst. Growth Des.* **2021**, *21* (6), 3438−3448.
(34) Shemchuk, O.; Grepioni, F.; Braga, D. Co-crystallization of racemic amino acids with ZnCl2: an investigation of chiral selectivity upon coordination to the metal centre. *CrystEngComm* **2020**, *22* (34), 5613−5619.
(35) Braga, D.; Degli Esposti, L.; Rubini, K.; Shemchuk, O.; Grepioni, F. Ionic Cocrystals of Racemic and Enantiopure Histidine: An Intriguing Case of Homochiral Preference. *Cryst. Growth Des.* **2016**, *16* (12), 7263−7270.
(36) Shemchuk, O.; Song, L.; Robeyns, K.; Braga, D.; Grepioni, F.; Leyssens, T. Solid-state chiral resolution mediated by stoichiometry: crystallizing etiracetam with ZnCl2. *Chem. Commun. (Camb)* **2018**, *54* (77), 10890−10892.
(37) Bravo, C.; Galego, F.; André, V. Hydrogen bonding networks of nalidixic acid−copper(ii) complexes. *CrystEngComm* **2019**, *21* (47), 7199−7203.

(38) Domingos, S.; Andre, V.; Quaresma, S.; Martins, I. C.; Minas da Piedade, M. F.; Duarte, M. T. New forms of old drugs: improving without changing. *J. Pharm. Pharmacol* **2015**, *67* (6), 830−846.
(39) Friščić, T.; Halasz, I.; Strobridge, F. C.; Dinnebier, R. E.; Stein, R. S.; Fábián, L.; Curfs, C. A rational approach to screen for hydrated forms of the pharmaceutical derivative magnesium naproxen using liquid-assisted grinding. *CrystEngComm* **2011**, *13* (9), 3125−3129.
(40) Friščić, T.; Fábián, L. Mechanochemical conversion of a metal oxide into coordination polymers and porous frameworks using liquid-assisted grinding (LAG). *CrystEngComm* **2009**, *11* (5), 743−745.
(41) Chow, E. H.; Strobridge, F. C.; Friscic, T. Mechanochemistry of magnesium oxide revisited: facile derivatisation of pharmaceuticals using coordination and supramolecular chemistry. *Chem. Commun. (Camb)* **2010**, *46* (34), 6368−6370.
(42) Yilmaz, V. T.; Topcu, Y.; Yilmaz, F.; Thoene, C. Saccharin complexes of Co(II), Ni(II), Cu(II), Zn(II), Cd(II) and Hg(II) with ethanolamine and diethanolamine: synthesis, spectroscopic and thermal characteristics. Crystal structures of $[Zn(ea)_2(sac)_2]$ and $[Cu_2(\mu\text{-dea})_2(sac)_2]$. *Polyhedron* **2001**, *20* (26−27), 3209−3217.
(43) Williams, P. A. M.; Ferrer, E. G.; Correa, M. J.; Baran, E. J.; Castellano, E. E.; Piro, O. E. Characterization of two new zinc(II) complexes with saccharinate and imidazole or benzimidazole as ligands. *Journal of Chemical Crystallography* **2004**, *34* (4), 285−290.
(44) Karabulut, B.; Ucar, I.; Koksal, F.; Yerli, Y. Crystal structure and EPR studies of doped Cu^{2+} ion in $[Zn(sac)_2(en)_2]$ single crystal. *Spectrochim Acta A Mol. Biomol Spectrosc* **2010**, *75* (4), 1195−1199.
(45) Herman, C.; Vermylen, V.; Norberg, B.; Wouters, J.; Leyssens, T. The importance of screening solid-state phases of a racemic modification of a chiral drug: thermodynamic and structural characterization of solid-state phases of etiracetam. *Acta Crystallogr. B Struct Sci. Cryst. Eng. Mater.* **2013**, *69* (4), 371−378.

https://doi.org/10.1021/acs.cgd.1c01462
Cryst. Growth Des. 2022, 22, 3016−3023